# Ion-Responsive 19F MRI Contrast Agents for the Detection of Cancer Cells

# Ion-responsive $^{19}$F MRI Contrast Agents for the Detection of Cancer Cells

Cheng Zhang,[1,2] Shehzahdi Shebbrin Moonshi,[1,2] Hui Peng,[1,2] Simon Puttick,[1,2] James Reid,[1] Stefano Bernardi,[1] Debra J. Searles,[1,3] Andrew K. Whittaker [1,2,4*]

[1] Australian Institute for Bioengineering and Nanotechnology, The University of Queensland, Brisbane Qld 4072

[2] ARC Centre of Excellence in Convergent Bio-Nano Science and Technology

[3] School of Chemistry and Molecular Biosciences, The University of Queensland, Brisbane Qld 4072

[4] Centre for Advanced Imaging, The University of Queensland, Brisbane Qld 4072

*Corresponding Author: Andrew K. Whittaker, a.whittaker@uq.edu.au*

*KEYWORDS: Ion-responsive, $^{19}$F NMR $T_2$, MD simulations, NOESY spectra, cancer detection*

**ABSTRACT:** Stimuli-responsive contrast agents (CAs) show great promise for the early detection and understanding of cancer. In particular, CAs that respond to ion content may allow monitoring of both the development of cancer and the efficacy of novel therapies. Understanding the responsive behaviour of stimuli-responsive CAs in different ionic environments requires development of more advanced characterization methods. Here we report a high-resolution NMR and molecular dynamics (MD) study of conformational changes of ion-responsive $^{19}$F co-polymers of oligo(ethylene glycol) methyl ether methacrylate (OEGMA) and 2,2,2-trifluoroethyl acrylate (TFEA) (poly(OEGMA-*co*-TFEA)) in the presence of salt. $^{1}$H 2D NOESY spectra were collected with and without the presence of NaCl and demonstrated that further separation of OEGMA and TFEA segments and closer association of OEGMA side chain were observed with the addition of NaCl. MD simulations provided additional information on the changes in conformation and were consistent with the experimental findings. Furthermore, we investigated the behaviour of polymer internalised by normal and cancer cells (MCF-12A and MCF-7) by monitoring the $^{19}$F spin-spin relaxation time ($T_2$) of poly(OEGMA-*co*-TFEA) copolymer *in vitro*. The $^{19}$F NMR $T_2$ values we obtained in MCF-7 cancer cells (82.3 ms) is much lower than that in MCF-12A normal cells (124.2 ms), and the difference is sufficient to obtain contrast using modern MRI methods in high field scanners. Our results encourage further attempts to develop even more potent CAs. This would also result in novel methods that allow monitoring of cancer at the cellular and molecular level.

Currently, one of the most important fields in biomedicine is the development of non-invasive imaging tools to support targeted therapies. Magnetic resonance imaging (MRI) plays a key role in the field because of its non-invasive nature, lack of radiation burden and in particular its capability to provide high resolution images with detailed anatomic contrast. There is increasing interest in the development of MRI techniques for the early detection of cancerous tissue, to enhance the survival rate and quality of life of cancer patients. However, the relative insensitivity of the MRI technique often requires the use of contrast agents (CAs).[1-3]

Over the past several decades numerous $^{1}$H MRI CAs, such as $Gd^{3+}$ and $Mn^{2+}$ chelates and superparamagnetic iron oxide (SPIO) particles have been developed and applied in pre-clinical and clinical settings.[4-8] Despite the wide-spread use of such $^{1}$H CAs, they retain several disadvantages. Principal amongst these is limited contrast due to the high background signal arising from the abundance of protons in tissue, making it difficult to distinguish tumour tissue from the surrounding normal tissue, especially at early stages of the disease. Furthermore, quantitative imaging using $^{1}$H based contrast agents is extremely challenging with generally a qualitative description of disease state being obtained.[9]

Recently $^{19}$F MRI has been championed by several groups as a promising alternative to $^{1}$H MRI because of its high sensitivity (83 % of $^{1}$H), high selectivity and more importantly, the lack of confounding background signal from the living body.[10-12] The experiment involves sequential acquisition of high-resolution proton density scans and $^{19}$F MR images, and superposition of the two scans in false color. This allows ready and unambiguous identification of the location of the fluorinated imaging agent. Furthermore, the total $^{19}$F signal intensity can be measured in a quantitative manner, and in the *in vivo* setting allows for tracking and counting of molecules or labelled cells.[13-15]

$^{19}$F MRI naturally relies on the use of fluorine-containing molecules or particles, and a high concentration of $^{19}$F nuclei is required in the target voxel to provide adequate signal for the acquisition of good quality images. The organic chemistry of fluorine is well established and it is known that fluorinated particles can provide a stable moiety for

interrogating many aspects of physiology and pharmacology *in vivo*. A range of fluorinated compounds, from small molecules to polymers, have been designed and studied as candidates of $^{19}$F MRI CAs.[16-21] Previous studies have indicated that polymeric $^{19}$F MRI agents are strong candidates for *in vivo* imaging, and accordingly several classes of polymeric agents have been prepared and tested.[9, 12, 20-27] The development of 'smart' CAs is a step further in the efforts to improve the specificity of MR imaging. So-called 'smart' CAs, which respond to changes in the microenvironment (ionic strength, pH, temperature, light, the presence of enzymes, redox potential, etc.), have created great interest.[12, 24, 28-30] In particular, the use of MRI to detect fluctuations in the concentration of vital ions has recently received much attention. Metcalfe and co-workers[31] synthesized a novel $^{19}$F NMR reporter, FCryp-1, to measure intracellular concentration of $Na^+$. A difference in $^{19}$F NMR chemical shift of 2 ppm between free FCryp-1 and Na-FCryp-1 complex provides a direct read out of free $Na^+$. More recently, Bulte and co-researchers[32] reported the detection of metal ions ($Ca^{2+}$) and discrimination between $Zn^{2+}$ and $Fe^{2+}$ using ion chemical exchange saturation transfer $^{19}$F MRI.

For the rational design of stimuli-responsive contrast agents to be optimised, a detailed understanding of the structure and dynamics of the polymeric agents is crucial. A combination of the nuclear Overhauser effect spectroscopy (NOESY) and molecular dynamics (MD) simulations recently reported by our group has been shown to be a promising method to study the conformational changes at molecular level in response to an external stimulus.[33, 34]

It is well known that compared to normal tissue, cancerous tissue can have a very different ionic composition. Thus it is suggested that normal and cancer tissue may be discriminated through selective imaging using CAs sensitive to ionic strength that are triggered by a change in concentration of ions. In the past few decades, it was reported by many researchers that the intracellular concentration of dissolved ions, especially sodium and chlorine, are elevated in cancer cells compared with normal cells.[35-39] Smith and co-workers[38] reported from energy-dispersive X-ray microanalysis that the concentrations of sodium and chlorine in transplantable H6 hepatoma cells in mice were more than double compared to the concentrations in normal hepatocytes. Similar results have been reported in other cancer cells.[40-42] More recently, Bertoni-Freddari and co-workers[43] studied the intracellular ratios of $Na^+$:$K^+$ in normal human and cancer cells and demonstrated that the high proliferating capacity of invasively growing cancer cells is accompanied by a significantly increased intranuclear and cytoplasmic $Na^+$:$K^+$ ratio due mostly to an increase content of sodium ions. These results indicate that detection of changes in intracellular ionic composition is a potential route to identification of cancerous cells.

Breast cancer is the most prevalent malignant disease threatening women worldwide. There is expectation that the survival rate can be improved with improved diagnostic screening methods for early-stage disease with reliable biomarkers.[44] The ionic composition of normal breast and cancer cells are also very different, based on measurements of mouse mammary tissue reported by Smith and co-workers.[39] These workers found that the sodium concentration is approximately three times higher in cancer cells compared with preneoplastic and normal mammary cells, the concentration of chlorine is twice as high while the potassium concentration is elevated in the cancer cells but not to the same extent.

In response to the need for imaging agents responsive to specific cell types, we have prepared partially-fluorinated statistical copolymers of oligo(ethylene glycol) methyl ether methacrylate (OEGMA) and 2,2,2-trifluoroethyl acrylate (TFEA) (poly(OEGMA-*co*-TFEA) copolymer) through reversible addition-fragmentation chain-transfer (RAFT) copolymerization. Previously we have reported the ion-responsive properties of these copolymers[45], however the mechanism of interaction of the salts with the copolymers remains to be elucidated. Herein we report a detailed study of the changes in conformation, microenvironment and $^{19}$F NMR relaxation times experienced by poly(OEGMA-*co*-TFEA) in the presence of dissolved salts, and complement these masurements with molecular dynamics (MD) simulations. The ion-responsive properties of these copolymers demonstrate their potential to be applied as indicators of cancerous cells. The poly(OEGMA-*co*-TFEA) copolymer was incubated with normal breast and cancer cells (MCF-12A and MCF-7, respectively) and changes in NMR properties including $^{19}$F NMR spin-spin relaxation times were measured. The results of this work provide direction for the design of ion-responsive $^{19}$F MRI contrast agents.

## EXPERIMENTAL SECTION

**Molecular Dynamics (MD) Simulations.** Fully atomistic models of poly(OEGMA-*co*-TFEA) consisting of 30 OEGMA and 10 TFEA repeat units were created and placed in a periodic simulation cell which was filled with water molecules at 298 K. Two sets of simulations were carried out: one is in water and the other is in salt solution. In the first case 22 000 water molecules were used, and for the second case the simulation was conducted in the presence of 1000 NaCl. The molecular system was built with chains initially in the fully extended state. The Materials Studio package was used to set up the initial structure and assign the force field parameters while MD simulations were carried out with the LAMMPS package.[46] The force field used for the current simulations was the CVFF force field with the SPC water model chosen to simulate the solvent.[47,48] Prior to data collection, the system was equilibrated for ~ 10 ns in a NPT (number of molecules (N), pressure (P), and temperature (T) are conserved) ensemble at 1 atm pressure. A Nosé-Hoover barostat and thermostat were used to constrain the pressure and temperature, respectively. Production runs were carried out for 30 ns with a time step of 1 fs. The radius of gyration and atomic positions were accumulated and stored every 1 ps.

**$^{19}$F NMR analysis of cellular uptake.** The $^{19}$F content per cell was determined by $^{19}$F NMR spectroscopy. For this, a large quantity of cells was required and cells were therefore grown in T75 flasks. The cell number was determined using a hemocytometer cell counter. Cells of a known

number were placed in 200 µl Triton lysis buffer (diluted in deuterium oxide) and mixed with 80 µl trifluoroacetic acid (TFA) $^{19}$F standard. Two distinct peaks were observed at -76.55 ppm for TFA and -73.9 ppm for the poly(OEGMA-*co*-TFEA) copolymer. The mean number of $^{19}$F nuclei per cell was calculated using the following formula: $F_c(^{19}F/Cells) = \frac{3I_s M_r N_a}{I_r N_c}$, Where the $I_s$ is integrated area of major peak of the cell pellet, $M_r$ is moles of TFA reference, $N_a$ is the Avogadro's number, $I_r$ is the integrated area under TFA reference peak and $N_c$ is the number of cells in pellet.

**Measurement of $^{19}$F NMR relaxation times.** Cells in three T175 flasks were cultured with the poly(OEGMA-*co*-TFEA) at a concentration of 20 mg/ml for 24 h and then fixed with 4 % paraformaldehyde *(*PFA) for 30 min. The samples were transferred into 3 mm NMR tubes and inserted into 5 mm NMR tubes filled with $D_2O$. The volume of the cells was sufficient to fill the detector region of the NMR coil, typically ~ 4 cm in length from the bottom of the NMR tube. Acquisition of $^{19}$F NMR spectrum and measurements of relaxation times $T_1$ & $T_2$ were carried on a Bruker Avance 400 MHz spectrometer.

$^{19}$F NMR spectra of the cells were acquired with a relaxation delay of 1 s, acquisition time of 1.26 s and the number of scans was 1024.

The $^{19}$F spin-spin ($T_2$) was measured using the Carr-Purcell-Meiboom-Gill (CPMG) pulse sequence at 310 K. The relaxation delay was 2 s, the acquisition time was 0.16 s and the number of scans was 512. For each measurement, the echo times (TE) were varied from 2 to 770 ms and 16 points were collected, which could be described by exponential functions for the calculation of $T_2$.

$^{19}$F spin-lattice ($T_1$) relaxation times were measured using the standard inversion-recovery pulse sequence. The relaxation delay was 2 s, the acquisition time was 0.16 s and the number of scans was 512. For each measurement, the recovery times were varied from 2 ms to 3 s and 16 points were acquired.

## RESULTS AND DISCUSSION

The central thesis to be examined in this work is that changes in ionic strength lead to changes in conformation and mobility of ion-responsive polymers in solution, which will further affect their NMR and MRI properties in a measurable manner. The aim of this study is therefore to assess the effects of ions on polymer conformation and dynamics at a molecular-level. The use of the ion-responsive poly(OEGMA-*co*-TFEA) copolymers for non-invasive detection of the normal and cancer cells will be examined. The statistical copolymer of OEGMA and TFEA ($F_{OEGMA}$ = 0.8) prepared using RAFT polymerization is a gradient copolymer with homogeneous chain-to-chain composition and its characterization was discussed in detail in our previous studies.[33, 45] The chemical structure of the copolymer is shown in Scheme 1. The detailed structural characteristics of the copolymer are summarized in Table S1 in the Supporting Information.

**Scheme 1. Schematic diagram illustrating the synthesis of poly(OEGMA-*co*-TFEA) copolymers via RAFT polymerization and the attachment with green fluorescence dye. The numbers in the structure corresponds to the assignments to the protons in the $^1$H NOESY NMR spectra.**

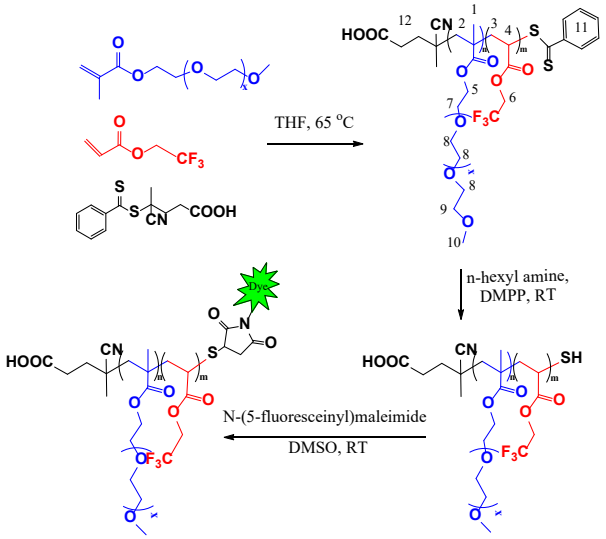


The effect of dissolved NaCl, a moderately strong salting-out species within the Hofmeister series, on polymer size in water solution was examined by dynamic light scattering (DLS). The number-average particle sizes of the poly(OEGMA-*co*-TFEA) copolymer and a homopolymer poly(OEGMA) were measured in pure water and in the presence of NaCl. Note that the number-average molecular weights of the copolymer and homopolymer, listed in Table S1 in the supporting information, are similar at around 20000 g/mol and 11000 g/mol from $^1$H NMR and SEC measurements, respectively. Both polymers have low molar mass dispersity. Several broad conclusions can be drawn from the results presented in Figure 1. First, the hydrodynamic diameters ($D_h$) of the polymers under all conditions are below 10 nm, indicating that the polymers are unimers in solution. Second, the $D_h$ of the poly(OEGMA-*co*-TFEA) copolymer is always significantly smaller than that of the poly(OEGMA) homopolymer. It is concluded that the hydrophobic TFEA segments in the copolymer result in water being a slightly less-good solvent; it is likely that the fluorinated segments associate, minimizing the contact with the solvent and the surface energy of the particle.[49, 50] As such, the introduction of the hydrophobic TFEA segments to the hydrophilic polymer of OEGMA units leads to a reduction in hydrodynamic diameter of the polymer. Third, the hydrodynamic diameter decreases on addition of NaCl, indicating the intramolecular self-association (the polymers remain as unimers in solution) of the ionic responsive polymers in the presence of salt.[51] To be more specific, the addition of ions to the solution leads to formation of ionic hydration layers around the polymer, and thus the hydrogen bonding structure of the polymer is broken down, which consequently is expected to lead to a reduction in the solvency of water for the polymer chains.[52-55]

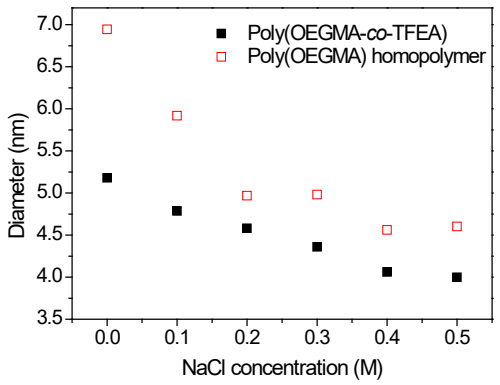


**Figure 1.** The hydrodynamic diameter ($D_h$) at 298 K of the poly(OEGMA) homopolymer and poly(OEGMA-*co*-TFEA) copolymer determined by DLS as a function of concentration of NaCl.

In an attempt to further understand the mechanism driving the ion-responsive behaviour of the poly(OEGMA-*co*-TFEA) copolymer, $^1$H NMR nuclear Overhauser effect spectroscopy ($^1$H NOESY) was conducted in pure water and in the presence of NaCl (0.1 M) at 298 K (Figure S1). The NOESY NMR experiment provides a powerful tool for the study of proximity of structures through space, typically over distances smaller than 5 Å.[56, 57] The cross-peak intensities in the NOESY spectra of the poly(OEGMA-*co*-TFEA) copolymer in $D_2O$ and a 0.1 M NaCl solution in $D_2O$ are summarized in Table S2. The cross-peak intensities which are most indicative of the changes in conformation of the poly(OEGMA-*co*-TFEA) copolymer are listed in Table 1.

The relative displacements of OEGMA and TFEA units are reflected by the changes of cross-peak intensities between protons 1 and 6, 5 and 6, 7 and 6 and 10 and 6. According to the data in Table 1, the cross-peak intensities of all of these pairs of protons are decreased on addition of NaCl, indicating an increase in average distance between OEGMA and TFEA segments. This can arise from the dehydration and aggregation of the hydrophilic OEGMA chains leading to the displacement of the OEGMA side chains from the TFEA units. Aggregation of the OEGMA side chains is also confirmed by increases in intensities of the cross-peaks between protons 7 and 10 and protons 8 and 10 from OEGMA segments (increases of 129 % and 66 %, respectively). However, the cross-peak intensities between protons 1 and 10 and protons 1 and 5 are slightly decreased by 26 % and 7 % (See Supporting Information Table S2). These observations indicate that the decrease in hydrodynamic diameter of the poly(OEGMA-*co*-TFEA) copolymer in the presence of NaCl is mainly due to aggregation of the OEGMA side chains with corresponding slight expansion of other segments of the copolymer. The mechanism driving the conformational changes of the copolymer in the presence of NaCl will be further discussed below.

To assist the interpretation of the experimental results, molecular dynamics (MD) simulations were performed on a single polymer chain of the poly(OEGMA-*co*-TFEA) copolymer at 298 K in water and in the presence of NaCl ions. MD simulations can provide powerful complimentary information on the conformational changes of specific segments of the copolymer at a molecular level. Initially, a poly(OEGMA-*co*-TFEA) copolymer chain consisting of 40 repeat units and composition consistent with the polymer examined by NMR (30 units of OEGMA and 10 units of TFEA) was constructed in pure water and in the presence of NaCl (12.4 wt %).[33] Prior to the collection of data, the system was equilibrated for ~10 ns. Subsequently, the conformation of the copolymer was simulated for ~30 ns with a time step of 1 fs. The radius of gyration ($R_g$) and atomic positions were accumulated and stored every 1 ps. Figure 2 shows the $R_g$ of the copolymer during 30 ns of simulation in water and with the addition of NaCl to the simulation box. The $R_g$ of the copolymer in the presence of NaCl is lower than that of the copolymer in water, which indicates that the conformation of the copolymer in pure water remains extended and well hydrated however the copolymer undergoes a conformation change to a folded 'dehydrated' state on the addition of NaCl. The reduction in $R_g$ in the "salt solution" is in excellent agreement with the DLS experimental studies.

The MD simulations also allow calculation of specific inter-atomic distances under the conditions considered. For example the average value of the shortest distance between the head and end of the OEGMA side chains (protons 7 to 10) was monitored at each time step. In pure water the average distance between protons 7 and 10 was 0.51 nm. However, in the presence of NaCl, the corresponding distance decreased to 0.45 nm, a reduction of 12 %. This observation is in accord with the NOESY results, indicating closer association of the OEGMA segments in the presence of the salt, contributing to the decrease in hydrodynamic radius of the copolymer. In order to compare the results of MD simulations with the experimental data, the calculations were not restricted to distances within single side chains, but averaged over the nearest proton pairs including inter-side chain contributions. It was noted that for the OEGMA side chains the shortest terminal-to-proximal distances were usually inter-chain distances (67 % and 90 % of the shortest distances are inter-chain in salt solution and pure water, respectively). Therefore the calculations provide a clear picture of changes in the conformation of the OEGMA side chains on a change in solvent quality, i.e. on addition of salt to the solution.

**Table 1. Cross-peak intensities in the NOESY spectra of the poly(OEGMA-*co*-TFEA) copolymer in $D_2O$ and 0.1 M NaCl $D_2O$ solutions. These values were calculated from the NOESY spectra by using the cross-peaks generated from the vicinal protons of H11 as an internal reference (the cross-peak intensity was set to 1). The proton numbering can be found in Scheme 1.**

| Protons | 1 to 6 | 5 to 6 | 7 to 6 | 10 to 6 | 7 to 10 | 8 to 10 |
|---|---|---|---|---|---|---|
| Poly(OEGMA-co-TFEA) copolymer in D2O | 2.55 | 2.94 | 1.29 | 1.05 | 1.13 | 2.86 |
| Poly(OEGMA-co-TFEA) copolymer in 0.1 M NaCl | 0.62 | 0.86 | 0.44 | 0.16 | 2.59 | 4.76 |

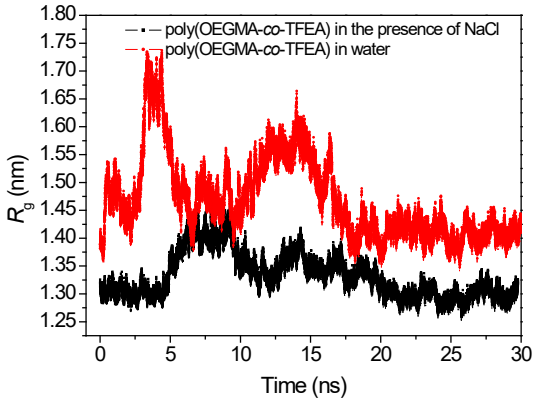


**Figure 2.** The radius of gyration ($R_g$) of the poly(OEGMA-*co*-TFEA) copolymer in pure water and in the presence of 12.4 wt % NaCl during a ~30 ns of simulation using LAMMPS at 298 K.

In addition to monitoring changes in the conformation of the OEGMA side chains, the behaviour of the fluorinated units was also monitored and averaged at each time step. Seven fluorine containing groups were included in the fictional polymer chain and placement based on the sequence distribution of the poly(OEGMA-*co*-TFEA) copolymer. On addition of salt to the simulation box the shortest distance between fluorine atoms decreased from 0.83 nm to 0.79 nm. This decrease in inter-nuclear separation is expected to lead to changes in the $^{19}$F NMR properties of the poly(OEGMA-*co*-TFEA) copolymer.

Figure 3 shows the structure of the poly(OEGMA-*co*-TFEA) copolymer at the end of a ~30 ns of simulation, in pure water an in salt solution. The copolymer clearly adopts a more extended conformation in pure water (Figure 3a) and a more globular conformation in the presence of NaCl (Figure 3b). These visual conformational changes are highly consistent with the decreases in $D_h$ and $R_g$ reported in Figure 1 and 2.

In order to further examine the behaviour of the polymer and other species in solution, the pair distribution functions, *g(r),* between the copolymer, water and ions were calculated. The results of NOESY and MD simulations indicate that the ion-responsive properties of the poly(OEGMA-*co*-TFEA) copolymer are heavily driven by the OEGMA side chains. Figure S2 shows the pair distribution functions between the ether oxygen atoms of the OEGMA side chain ($O_1$) and oxygen and hydrogen atoms of $H_2O$ in water and salt solution. The intensities of the first peak in *g(r)* between the $O_1$ atoms and water atoms are significantly higher in pure water than in salt solution (Figure S2).[58] This indicates that the interactions between $O_1$ atoms and water are reduced and the solvency of water for the polymer chains is decreased on addition of NaCl. Clearly the distribution of water molecules around the $O_1$ atoms is strongly affected by the addition of NaCl.

The MD simulations of the poly(OEGMA-*co*-TFEA) copolymer in the presence of NaCl (Figure 4c), also revealed the existence of two different types of $O_1$ atoms in the OEGMA ether side chain. These are $O_1$ atoms closely associated with $Na^+$ ions (labelled $O_{1a}$), and $O_1$ atoms which predominantly interact with water molecules (these are labelled $O_{1b}$). The former of these, $O_{1a}$, are illustrated closely associated with $Na^+$ ions in the snapshot from the simulation in Figure 4c). The pair distribution functions for $O_{1a}$ and water shown in Figure 4a reveal the absence of a peak in $g(r_{O_{1a}:H})$ within a diameter of 4 Å, and a broad peak in $g(r_{O_{1a}:O})$ at ~ 3.4 Å. This indicates that $O_{1a}$ atoms and water do not form strong hydrogen bonds. The peak located at ~ 3.4 Å in $g(r_{O_{1a}:O})$ arises from water bonded directly with $Na^+$ ions; the $Na^+$ ions interact directly with $O_{1a}$ leading to a partial dehydration of the copolymer. The water molecules around the $Na^+$ ions are oriented by the ionic field (ion hydration), and more specifically the affinity between the $Na^+$ and O atoms of $H_2O$ is much stronger than that between the $Na^+$ and H atoms of $H_2O$ (see Figure S3 in Supporting Information). The other type of $O_1$ (namely $O_{1b}$), shows strong affinity with both O and H atoms of $H_2O$ as shown in Figure 4b, and provide partial hydration of the copolymer. These results indicate that partial hydration/dehydration of the copolymer, ion hydration and direct interactions between ions and the copolymer all drive the conformational changes of the poly(OEGMA-*co*-TFEA) copolymer in salt solution, and provides a clear understanding of the well-known 'salting-out' effect of PEG-containing systems. [55, 59-61]

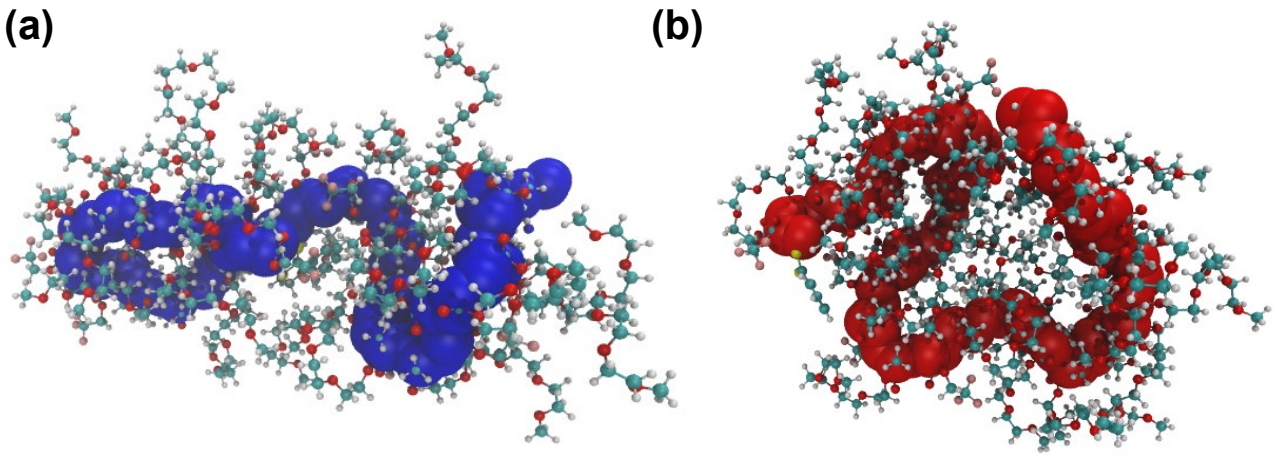


**Figure 3.** Snapshots of the poly(OEGMA-*co*-TFEA) chains taken at the end of a ~30 ns simulation in (a) pure water (backbone carbon atoms are shown in blue) and (b) in salt solution (12.4 wt % NaCl) (backbone carbon atoms are shown in red). Water molecules and NaCl ions have been omitted for clarity.

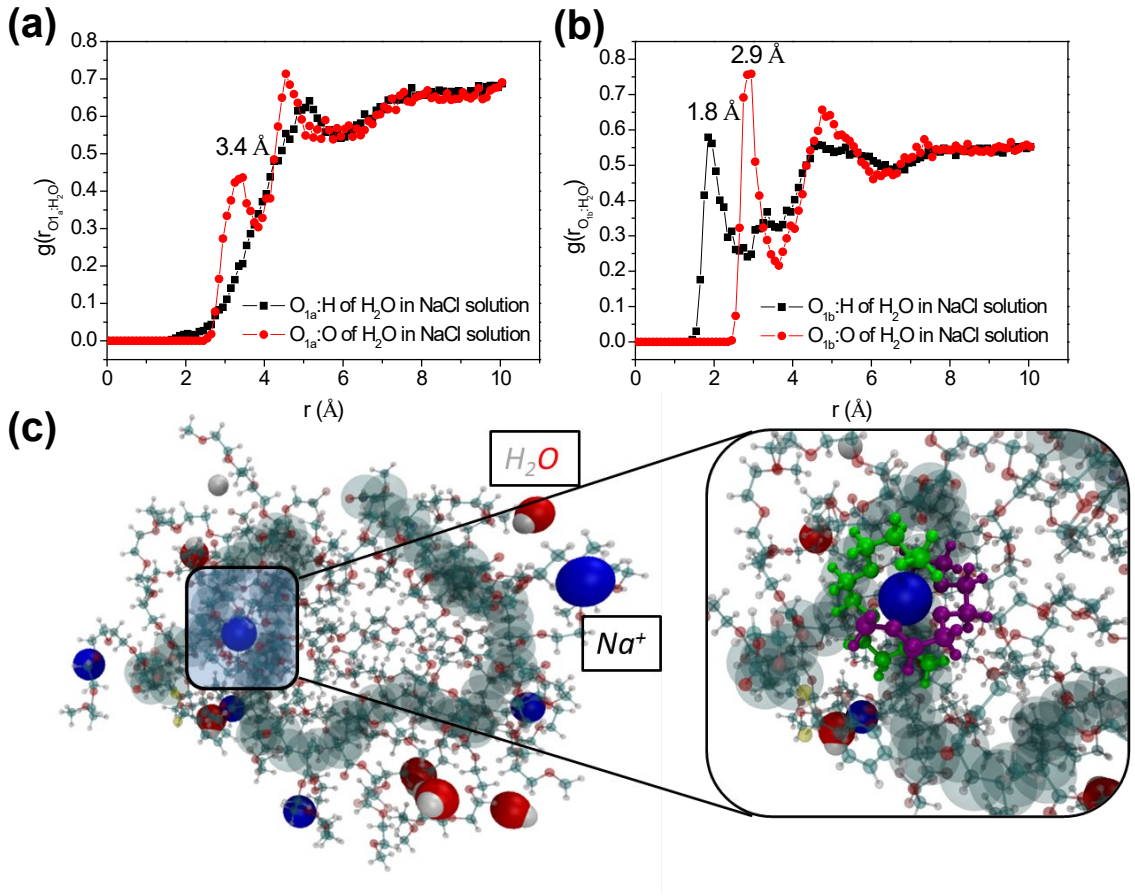


**Figure 4.** The interactions between NaCl and the poly(OEGMA-*co*-TFEA) copolymer in the presence of 12.4 wt % NaCl. (a) and (b) The pair distribution functions *g(r)* of the $O_{1a}$ and $O_{1b}$ atoms of OEGMA side chains to H and O atoms of $H_2O$. (c) A snapshot from the MD simulations showing the distribution of water and ions within 4 Å of the copolymer.

We propose that the poly(OEGMA-*co*-TFEA) copolymer can act as an ion-responsive $^{19}F$ MRI contrast agent on the basis of the studies escribed above of the conformational changes in salt solution. Our previous studies of partially-fluorinated polymers show that the performance of this class of macromolecule as $^{19}F$ MRI agents depends on structural parameters such as the number of fluorine spins, and dynamic parameter, namely the longitudinal and transverse relaxation times ($^{19}F$ $T_1$ and $T_2$).[62] For these systems the spin-spin relaxation time ($T_2$), which is determined by the strength of the dipolar coupling of the $^{19}F$ nuclei with

near-neighbour fluorine and proton nuclei, is most important in determining MRI performance. The value of $T_2$ is highly sensitive to the spatial arrangement of the nuclear spins and their relative mobility, parameters which are very sensitive to the polymer conformation.

It is clear that changes in the $^{19}$F NMR $T_2$ can serve as an indicator for the changes in microenvironment of the $^{19}$F spins in solution. The sensitivity of the copolymer to salt solution was examined by measurement of the $^{19}$F NMR $T_2$ in aqueous solutions of NaCl at 310 K. As can be seen in Figure 5 the $^{19}$F NMR $T_2$ decreased with an increase in concentration of NaCl in solution. Note that the concentration range spans the range of physiological ionic strengths found in the body. The observed decrease in $T_2$ can be rationalised by reference to the results of NOESY measurements and MD simulations presented in the previous section. Partial dehydration of the poly(OEGMA-*co*-TFEA) copolymer in the salt solution leads to a reduction in chain dimensions ($R_g$) and closer association of the TFEA segments. The combination of reduced homo- and hetero-nuclear separation and a likely decrease in intramolecular segmental mobility on partial chain collapse, leads to an increase in the strength of the dipolar couplings and, as such, a reduced $^{19}$F $T_2$ relaxation time. The $^{19}$F NMR $T_1$ relaxation times of the copolymer were measured in solutions at different concentrations of NaCl and found not to change substantially indicating no substantial change in the high frequency motions of the trifluoromethyl group in TFEA (Table S3).

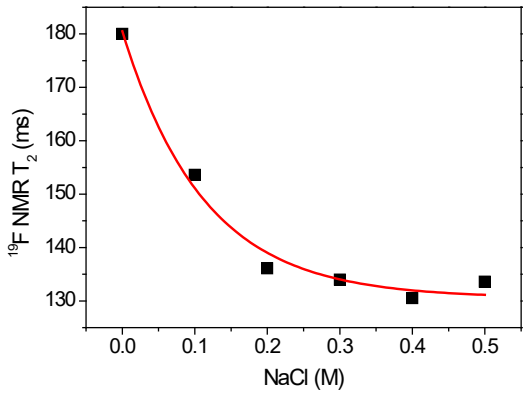


**Figure 5.** $^{19}$F NMR $T_2$ relaxation times for the poly(OEGMA-*co*-TFEA) copolymer in deionized water and in NaCl solutions (0.1 M to 0.5 M) at 310 K measured at a field strength of 9.4 T.

An *in vitro* examination of the ion-responsive behaviour of the copolymers was conducted by incubation of solutions of the copolymer with normal and cancer cells. Prior to this the copolymer was further modified by conjugation with *N*-(5-fluoresceinyl)maleimide as a fluorescent reporter. The cellular uptake of the poly(OEGMA-*co*-TFEA)-Mal*N*Flu copolymer was studied by fluorescence microscopy and $^{19}$F NMR spectroscopy. As shown in Figure S4a, cells treated with the copolymer demonstrated significant amount green fluorescence, mostly within the cytoplasm indicating successful cellular uptake.

Cytocompatibility is a key concern for materials to be used in biomedical applications.[63,64] As such, we investigated the cytocompatibility of the poly(OEGMA-*co*-TFEA)-Mal*N*Flu copolymer with MCF-7 and MCF-12A cells via a MTS cell viability assay (Figure S4b and Figure S6). The copolymer does not display apparent cytotoxicity in the concentration from 1 to 20 mg/ml after incubation for 24 h. This demonstrates that these fluorine-containing copolymers do not significantly impact the viability of the cells.

$^{19}$F NMR spectroscopy was also employed to confirm and quantify cell uptake of the poly(OEGMA-*co*-TFEA)-Mal*N*Flu copolymer. A major peak in the spectrum at ~ -73.9 ppm was observed due to poly(OEGMA-*co*-TFEA) copolymer. Trifluoroacetic acid (TFA, -76.55 ppm) was used as an internal reference to quantify the number of fluorine spins per cell (Figure S7). Using the method reported by Ahrens and co-workers[15], we measured a $^{19}$F content in each cell of approximately 1.45 x $10^{10}$ fluorine spins.

The $^{19}$F NMR $T_2$ of the poly(OEGMA-*co*-TFEA) copolymer was measured after uptake into normal breast cells and breast cancer cells (MCF-12A and MCF-7, respectively). As the intracellular concentration of salt is significantly different in these cells[39], it is postulated that differences in conformation of the copolymer will be reflected in the $^{19}$F NMR $T_2$ of the copolymer. The cells were incubated with the poly(OEGMA-*co*-TFEA) copolymer for 24 h and fixed with 4 % paraformaldehyde followed by centrifugation to form a pellet. To prevent the contamination of the cells with the deuterated solvent, $D_2O$ was added to a 5 mm NMR tube to provide the lock signal. The cell pellet was added into an insert tube (3 mm outer diameter) which was placed into the standard 5 mm NMR tube containing the $D_2O$.[65] Figure 6a shows the $^{19}$F NMR spectra at 301 K of the copolymer in water, and within normal and cancer cells (MCF-12A and MCF-7). The small peak at 73.2 ppm, which is assigned to long sequences of TFEA units in the copolymer,[33] was not apparent in the spectra of MCF-7 cells. This is ascribed to aggregation of polymer segments, in particular the highly-fluorinated parts, in cancer cells having higher ionic content, leading to prohibitively short $T_2$ relaxation times for those groups.[45]

The results of measurements of $^{19}$F NMR $T_2$ relaxation times of the poly(OEGMA-*co*-TFEA) copolymer in MCF-7 and MCF-12A cells are shown in Figure 6b. The $^{19}$F NMR $T_2$ of the copolymer in pure water was 178 ms, while this dropped to 124 and 82 ms in MCF-12A cells and MCF-7 cancer cells, respectively. This is clear demonstration that the copolymer is undergoing changes in conformation, confirmed by the experimental and computational studies, in the cells, and that this is reflected in the lower values of $^{19}$F $T_2$ relaxation times. Importantly the elevated salt content in the cancer cells (MCF-7) leads to a significantly lower relaxation time compared with the healthy cells (MCF-12A). The potential for these copolymers to act as indicators of cellular ionic strength is clearly demonstrated by this study.

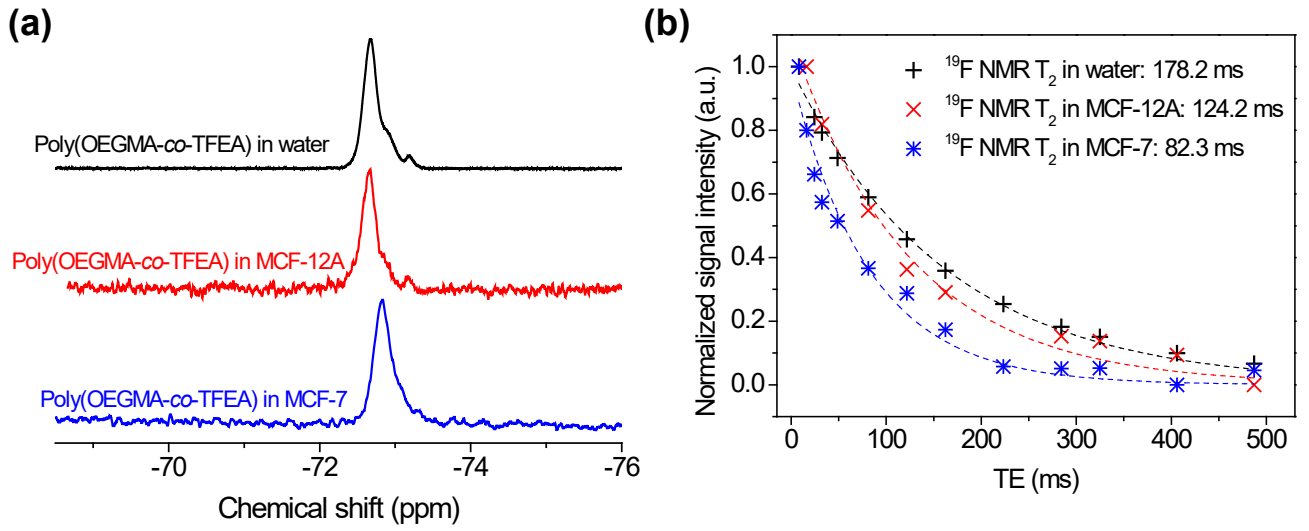


**Figure 6.** *In vitro* $^{19}$F NMR measurements. (a) $^{19}$F NMR spectra of the poly(OEGMA-*co*-TFEA) copolymer in water, MCF-12A normal cells and MCF-7 cancer cells. The multiple peaks in the $^{19}$F NMR spectrum arise from different sequences of TFEA in the copolymer. (b) $^{19}$F NMR $T_2$ relaxation curves and fits to exponential decays for the copolymer in water, normal breast (MCF-12A) and cancer cells (MCF-7).

## CONCLUSIONS

In summary, we have reported a novel ion-responsive copolymer of OEGMA and TFEA prepared through RAFT polymerization. Detailed and systematic studies of the changes in conformation and mobility of the poly(OEGMA-*co*-TFEA) copolymer in aqueous and salt solutions were conducted. The hydrodynamic diameter ($D_h$) of the copolymer was measured by DLS and found to decrease on addition of NaCl to the solution. $^1$H 2D NOESY and MD simulations indicate that OEGMA side chains tended to undergo inter-side chain association and that the displacement with respect to the main chain decreased. MD simulations show that a $Na^+$ ions were closely with the ether oxygen atoms of many OEGMA side chains, driving a partial dehydration of the poly(OEGMA-*co*-TFEA) copolymer. The ion-responsive nature of the copolymer was exploited as a non-invasive indicator of cancer cells. The poly(OEGMA-*co*-TFEA) copolymer was incubated with normal breast and cancer cells (MCF-12A and MCF-7, respectively) and the $^{19}$F NMR $T_2$ relaxation time in the cancer cells found to be significantly lower than that in normal cells. These results indicate that the $^{19}$F NMR $T_2$ relaxation time of these polymers can serve as a valuable and robust marker for detection of cancer tissue.

## ASSOCIATED CONTENT

**Supporting Information**. Supporting Information Available: The following files are available free of charge. Materials, characterizations, synthesis of the copolymer, cell culture, $^1$H 2D NOESY spectra, the cross peak intensities calculated from NOESY spectra, pair distribution functions, fluorescence microscope images, MTS assay and $^{19}$F NMR spectrum of the copolymer in normal cells.

## AUTHOR INFORMATION


### Corresponding Author

* a.whittaker@uq.edu.au


### Notes

The authors declare no competing financial interest.

## ACKNOWLEDGMENTS


The authors acknowledge the Australian Research Council (CE140100036, DP0987407, DP110104299, LE0775684, LE0668517, and LE0882357) and the National Health and Medical Research Council (APP1021759) for funding of this research. The Australian National Fabrication Facility, Queensland Node, is also acknowledged for access to some items of equipment. Dr. Hui Peng thanks the University of Queensland for her UQ Postdoctoral Research Fellowship for Women. This research was undertaken with support from the Queensland Cyber Infrastructure Foundation (QCIF) and the University of Queensland Research Computing Centre.


## REFERENCES


(1) Li, X.; Qian, Y.; Liu, T.; Hu, X.; Zhang, G.; You, Y.; Liu, S. Amphiphilic multiarm star block copolymer-based multifunctional unimolecular micelles for cancer targeted drug delivery and MR imaging. Biomaterials **2011**, *32*, 6595-6605.

(2) Li, Y.; Yu, H.; Qian, Y.; Hu, J.; Liu, S. Amphiphilic Star Copolymer-Based Bimodal Fluorogenic/Magnetic Resonance Probes for Concomitant Bacteria Detection and Inhibition. Adv. Mater. **2014**, *26*, 6734-6741.

(3) Hu, X.; Liu, G.; Li, Y.; Wang, X.; Liu, S. Cell-Penetrating Hyperbranched Polyprodrug Amphiphiles for Synergistic Reductive Milieu-Triggered Drug Release and Enhanced Magnetic Resonance Signals. J. Am. Chem. Soc. **2015**, *137*, 362-368.

(4) Mishra, A.; Fousková, P.; Angelovski, G.; Balogh, E.; Mishra, A. K.; Logothetis, N. K.; Tóth, É. Facile Synthesis and Relaxation Properties of Novel Bispolyazamacrocyclic $Gd^{3+}$ Complexes: An

Attempt towards Calcium-Sensitive MRI Contrast Agents. *Inorg. Chem.* **2008**, *47*, 1370-1381.

(5) Richard, C.; Doan, B.-T.; Beloeil, J.-C.; Bessodes, M.; Tóth, É.; Scherman, D. Noncovalent Functionalization of Carbon Nanotubes with Amphiphilic $Gd^{3+}$ Chelates: Toward Powerful T1 and T2 MRI Contrast Agents. *Nano Lett.* **2008**, *8*, 232-236.

(6) Molnár, E.; Camus, N.; Patinec, V.; Rolla, G. A.; Botta, M.; Tircsó, G.; Kálmán, F. K.; Fodor, T.; Tripier, R.; Platas-Iglesias, C. Picolinate-Containing Macrocyclic $Mn^{2+}$ Complexes as Potential MRI Contrast Agents. *Inorg. Chem.* **2014**, *53*, 5136-5149.

(7) Jin, H.; Liu, S.; Guo, F.; Zhang, B. Polymer-Coated Superparamagnetic Iron Oxide Nanoparticles: Synthesis, Characterization and Toxicity Evaluation for MRI in Mice. *J. Biomater. Tissue Eng.* **2014**, *4*, 443-449.

(8) Tsai, Z.-T.; Wang, J.-F.; Kuo, H.-Y.; Shen, C.-R.; Wang, J.-J.; Yen, T.-C. In situ preparation of high relaxivity iron oxide nanoparticles by coating with chitosan: A potential MRI contrast agent useful for cell tracking. *J. Magn. Magn. Mater.* **2010**, *322*, 208-213.

(9) Knight, J. C.; Edwards, P. G.; Paisey, S. J. Fluorinated contrast agents for magnetic resonance imaging; a review of recent developments. *RSC Adv.* **2011**, *1*, 1415-1425.

(10) Janjic, J. M.; Ahrens, E. T. Fluorine-containing nanoemulsions for MRI cell tracking. *Wiley Interdiscip. Rev. Nanomed. Nanobiotechnol.* 2009, *1*, 492-501.

(11) Ruiz-Cabello, J.; Barnett, B. P.; Bottomley, P. A.; Bulte, J. W. M. Fluorine ($^{19}F$) MRS and MRI in biomedicine. *NMR Biomed.* **2011**, *24*, 114-129.

(12) Wang, K.; Peng, H.; Thurecht, K. J.; Puttick, S.; Whittaker, A. K. Biodegradable core crosslinked star polymer nanoparticles as $^{19}F$ MRI contrast agents for selective imaging. *Polym. Chem.* **2014**, *5*, 1760-1771.

(13) Srinivas, M.; Heerschap, A.; Ahrens, E. T.; Figdor, C. G.; Vries, I. J. M. d. $^{19}F$ MRI for quantitative in vivo cell tracking. *Trends Biotechnol.* **2010**, *28*, 363-370.

(14) Ahrens, E. T.; Zhong, J. In vivo MRI cell tracking using perfluorocarbon probes and fluorine-19 detection. *NMR Biomed.* **2013**, *26*, 860-871.

(15) Ahrens, E. T.; Helfer, B. M.; O'Hanlon, C. F.; Schirda, C. Clinical cell therapy imaging using a perfluorocarbon tracer and fluorine-19 MRI. *Magn. Reson. Med.* **2014**, *72*, 1696-1701.

(16) Joseph, P. M.; Yuasa, Y.; Kundel, H. L.; Mukherji, B.; Sloviter, H. A. Magnetic resonance imaging of fluorine in rats infused with artificial blood. *Invest. Radiol.* **1985**, *20*, 504-509.

(17) Mason, R. P.; Bansal, N.; Babcock, E. E.; Nunnally, R. L.; Antich, P. P. A novel editing technique for $^{19}F$ MRI: Molecule-specific imaging. *Magn. Reson. Imaging* **1990**, *8*, 729-736.

(18) Mengna, X.; Vikram, K.; Hanli, L.; Ralph, P. M. Tumour oxygen dynamics measured simultaneously by near-infrared spectroscopy and $^{19}$ F magnetic resonance imaging in rats. *Phys. Med. Biol.* **2006**, *51*, 45.

(19) Jacoby, C.; Temme, S.; Mayenfels, F.; Benoit, N.; Krafft, M. P.; Schubert, R.; Schrader, J.; Flögel, U. Probing different perfluorocarbons for in vivo inflammation imaging by 19F MRI: image reconstruction, biological half-lives and sensitivity. *NMR Biomed.* **2014**, *27*, 261-271.

(20) Díaz-López, R.; Tsapis, N.; Fattal, E. Liquid Perfluorocarbons as Contrast Agents for Ultrasonography and $^{19}F$-MRI. *Pharm. Res.* **2010**, *27*, 1-16.

(21) Peng, H.; Blakey, I.; Dargaville, B.; Rasoul, F.; Rose, S.; Whittaker, A. K. Synthesis and Evaluation of Partly Fluorinated Block Copolymers as MRI Imaging Agents. *Biomacromolecules* **2009**, *10*, 374-381.

(22) Huang, X.; Huang, G.; Zhang, S.; Sagiyama, K.; Togao, O.; Ma, X.; Wang, Y.; Li, Y.; Soesbe, T. C.; Sumer, B. D.; Takahashi, M.; Sherry, A. D.; Gao, J. Multi-Chromatic pH-Activatable $^{19}F$-MRI Nanoprobes with Binary ON/OFF pH Transitions and Chemical-Shift Barcodes. *Angew. Chem. Int. Ed.* **2013**, *52*, 8074-8078.

(23) Du, W.; Nyström, A. M.; Zhang, L.; Powell, K. T.; Li, Y.; Cheng, C.; Wickline, S. A.; Wooley, K. L. Amphiphilic Hyperbranched Fluoropolymers as Nanoscopic $^{19}F$ Magnetic Resonance Imaging Agent Assemblies. *Biomacromolecules* **2008**, *9*, 2826-2833.

(24) Wang, K.; Peng, H.; Thurecht, K. J.; Puttick, S.; Whittaker, A. K. pH-responsive star polymer nanoparticles: potential $^{19}F$ MRI contrast agents for tumour-selective imaging. *Polym. Chem.* **2013**, *4*, 4480-4489.

(25) Thurecht, K. J.; Blakey, I.; Peng, H.; Squires, O.; Hsu, S.; Alexander, C.; Whittaker, A. K. Functional Hyperbranched Polymers: Toward Targeted in Vivo $^{19}F$ Magnetic Resonance Imaging Using Designed Macromolecules. *J. Am. Chem. Soc.* **2010**, *132*, 5336-5337.

(26) Nurmi, L.; Peng, H.; Seppala, J.; Haddleton, D. M.; Blakey, I.; Whittaker, A. K. Synthesis and evaluation of partly fluorinated polyelectrolytes as components in $^{19}F$ MRI-detectable nanoparticles. *Polym. Chem.* **2010**, *1*, 1039-1047.

(27) Ogawa, M.; Nitahara, S.; Aoki, H.; Ito, S.; Narazaki, M.; Matsuda, T. Fluorinated Polymer Nanoparticles as a Novel $^{19}F$ MRI Contrast Agent Prepared by Dendrimer-Initiated Living Radical Polymerization. *Macromol. Chem. Phys.* **2010**, *211*, 1369-1376.

(28) Himmelreich, U.; Aime, S.; Hieronymus, T.; Justicia, C.; Uggeri, F.; Zenke, M.; Hoehn, M. A responsive MRI contrast agent to monitor functional cell status. *NeuroImage* **2006**, *32*, 1142-1149.

(29) Ali, M. M.; Woods, M.; Caravan, P.; Opina, A. C. L.; Spiller, M.; Fettinger, J. C.; Sherry, A. D. Synthesis and Relaxometric Studies of a Dendrimer-Based pH-Responsive MRI Contrast Agent. *Chem. Eur. J.* **2008**, *14*, 7250-7258.

(30) Tóth, É.; Bolskar, R. D.; Borel, A.; González, G.; Helm, L.; Merbach, A. E.; Sitharaman, B.; Wilson, L. J. Water-Soluble Gadofullerenes: Toward High-Relaxivity, pH-Responsive MRI Contrast Agents. *J. Am. Chem. Soc.* **2005**, *127*, 799-805.

(31) Smith, G. A.; Morris, P. G.; Hesketh, T. R.; Metcalfe, J. C. Design of an indicator of intracellular free $Na^+$ concentration using 19 F-NMR. *Biochim. Biophys. Acta* **1986**, *889*, 72-83.

(32) Bar-Shir, A.; Yadav, N. N.; Gilad, A. A.; van Zijl, P. C. M.; McMahon, M. T.; Bulte, J. W. M. Single $^{19}F$ Probe for Simultaneous Detection of Multiple Metal Ions Using miCEST MRI. *J. Am. Chem. Soc.* **2015**, *137*, 78-81.

(33) Zhang, C.; Peng, H.; Puttick, S.; Reid, J.; Bernardi, S.; Searles, D. J.; Whittaker, A. K. Conformation of Hydrophobically Modified Thermoresponsive Poly(OEGMA-co-TFEA) across the LCST Revealed by NMR and Molecular Dynamics Studies. *Macromolecules* **2015**, *48*, 3310-3317.

(34) Zhang, C.; Peng, H.; Li, W.; Liu, L.; Puttick, S.; Reid, J.; Bernardi, S.; Searles, D. J.; Zhang, A.; Whittaker, A. K. Conformation Transitions of Thermoresponsive Dendronized Polymers across the Lower Critical Solution Temperature. *Macromolecules* **2016**, *49*, 900-908.

(35) Cameron, I. L.; Smith, N. K. R.; Pool, T. B.; Sparks, R. L. Intracellular Concentration of Sodium and Other Elements as Related to Mitogenesis and Oncogenesis in Vivo. *Cancer Res.* **1980**, *40*, 1493-1500.

(36) Zs.-Nagy, I.; Lustyik, G.; Lukács, G.; Zs.-Nagy, V.; Balázs, G. Correlation of Malignancy with the Intracellular $Na^+$:$K^+$ Ratio in Human Thyroid Tumors. *Cancer Res.* **1983**, *43*, 5395-5402.

(37) Despa, S.; Islam, M. A.; Weber, C. R.; Pogwizd, S. M.; Bers, D. M. Intracellular $Na^+$ concentration is elevated in heart failure but Na/K pump function is unchanged. *Circulation* **2002**, *105*, 2543-2548.

(38) Smith, N. R.; Sparks, R. L.; Pool, T. B.; Cameron, I. L. Differences in the Intracellular Concentration of Elements in Normal and Cancerous Liver Cells as Determined by X-ray Microanalysis. *Cancer Res.* **1978**, *38*, 1952-1959.

(39) Smith, N. K. R.; Stabler, S. B.; Cameron, I. L.; Medina, D. X-Ray Microanalysis of Electrolyte Content of Normal, Preneoplastic, and Neoplastic Mouse Mammary Tissue. *Cancer Res.* **1981**, *41*, 3877-3880.

(40) Cameron, I. L.; Pool, T. B.; Smith, N. K. R. An X-ray microanalysis survey of the concentration of elements in the cytoplasm of different mammalian cell types. *J. Cell. Physio.* **1979**, *101*, 493-501.

(41) Cameron, I. L.; Smith, N. K.; Pool, T. B. Element concentration changes in mitotically active and postmitotic enterocytes. An x-ray microanalysis study. *J. Cell Biol.* **1979**, *80*, 444-450.

(42) Cameron, I.; Smith, N. Energy dispersive x-ray microanalysis of the concentration of elements in relation to cell reproduction in normal and in cancer cells. *Scan. Electron Micros.* **1980**, 463.

(43) Nagy, I. Z.; Lustyik, G.; Nagy, V. Z.; Zarándi, B.; Bertoni-Freddari, C. Intracellular $Na^+$:$K^+$ ratios in human cancer cells as revealed by energy dispersive x-ray microanalysis. *J. Cell Biol.* **1981**, *90*, 769-777.

(44) Jemal, A.; Siegel, R.; Ward, E.; Hao, Y.; Xu, J.; Thun, M. J. Cancer Statistics, 2009. *CA-Cancer J. Clin.* **2009**, *59*, 225-249.

(45) Zhang, C.; Peng, H.; Whittaker, A. K. NMR investigation of effect of dissolved salts on the thermoresponsive behavior of oligo(ethylene glycol)-methacrylate-based polymers. *J. Polym. Sci., Part A: Polym. Chem.* **2014**, *52*, 2375-2385.

(46) Chandler, D. Interfaces and the driving force of hydrophobic assembly. *Nature* **2005**, *437*, 640-647.

(47) Mikheev, Y. A.; Guseva, L. N.; Davydov, E. Y.; Ershov, Y. A. The hydration of hydrophobic substances. *Russ. J. Phys. Chem. A* **2007**, *81*, 1897-1913.

(48) Tan, B. H.; Tam, K. C.; Lam, Y. C.; Tan, C. B. Microstructure and Rheology of Stimuli-Responsive Nanocolloidal SystemsEffect of Ionic Strength. *Langmuir* **2004**, *20*, 11380-11386.

(49) Erlander, S. R. Interaction of Aqueous Ions: A Correlation between the Hydration and Solubility Properties of Inorganic, Organic, and Polymeric Salts Having Mono- or Polyatomic Ions. *J. Macromol. Sci. Chem.* **1968**, *2*, 623-643.

(50) Erlander, S. R. Determination of the Structure and Effective Dielectric Constant of Hydrated Ions. *J. Macromol. Sci. Chem.* **1968**, *2*, 833-858.

(51) Erlander, S. R. Explanation of Ionic Sequences in Various Phenomena. I. Salting-Out of Uncharged Molecules. *J. Macromol. Sci. Chem.* **1968**, *2*, 1065-1072.

(52) Thormann, E. On understanding of the Hofmeister effect: how addition of salt alters the stability of temperature responsive polymers in aqueous solutions. *RSC Adv.* **2012**, *2*, 8297-8305.

(53) Mumenthaler, C.; Braun, W. Automated Assignment of Simulated and Experimental NOESY Spectra of Proteins by Feedback Filtering and Self-correcting Distance Geometry. *J. Mol. Biol.* **1995**, *254*, 465-480.

(54) Banks, K. M.; Hare, D. R.; Reid, B. R. Three-dimensional solution structure of a DNA duplex containing the BclI restriction sequence: two-dimensional NMR studies, distance geometry calculations, and refinement by back-calculation of the NOESY spectrum. *Biochemistry* **1989**, *28*, 6996-7010.

(55) Du, H.; Wickramasinghe, R.; Qian, X. Effects of salt on the lower critical solution temperature of poly (N-isopropylacrylamide). *J. Phys. Chem. B* **2010**, *114*, 16594-16604.

(56) Florin, E.; Kjellander, R.; Eriksson, J. C. Salt effects on the cloud point of the poly(ethylene oxide)+water system. *J. Chem. Soc., Faraday Trans. 1* **1984**, *80*, 2889-2910.

(57) Zhang, Y.; Furyk, S.; Sagle, L. B.; Cho, Y.; Bergbreiter, D. E.; Cremer, P. S. Effects of Hofmeister Anions on the LCST of PNIPAM as a Function of Molecular Weight. *J. Phys. Chem. C* **2007**, *111*, 8916-8924.

(58) Zhang, Y.; Furyk, S.; Bergbreiter, D. E.; Cremer, P. S. Specific Ion Effects on the Water Solubility of Macromolecules: PNIPAM and the Hofmeister Series. *J. Am. Chem. Soc.* **2005**, *127*, 14505-14510.

(59) Hendrick, R. E.; Kneeland, J. B.; Stark, D. D. Maximizing signal-to-noise and contrast-to-noise ratios in flash imaging. *Magn. Reson. Imaging* **1987**, *5*, 117-127.

(60) Wang, H.; Zheng, L.; Peng, C.; Guo, R.; Shen, M.; Shi, X.; Zhang, G. Computed tomography imaging of cancer cells using acetylated dendrimer-entrapped gold nanoparticles. *Biomaterials* **2011**, *32*, 2979-2988.

(61) Liu, H.; Wang, H.; Xu, Y.; Shen, M.; Zhao, J.; Zhang, G.; Shi, X. Synthesis of PEGylated low generation dendrimer-entrapped gold nanoparticles for CT imaging applications. *Nanoscale* **2014**, *6*, 4521-4526.

(62) Hammill, J. T.; Miyake-Stoner, S.; Hazen, J. L.; Jackson, J. C.; Mehl, R. A. Preparation of site-specifically labeled fluorinated proteins for 19F-NMR structural characterization. *Nat. Protoc.* **2007**, *2*, 2601-2607.

(63) Plimpton, S. Fast Parallel Algorithms for Short-Range Molecular Dynamics. *J. Comp. Phys.* **1995**, 117, 1-19.

(64) Berendsen, H.; Postma, J.; Van Gunsteren, W.; Hermans, J. Intermolecular Forces, ed Pullman B. D Reidel Publishing Company, Dordrecht, The Netherlands: **1981**; pp 331-342.

(65) Dauber-Osguthorpe, P.; Roberts, V. A.; Osguthorpe, D. J.; Wolff, J.; Genest, M.; Hagler, A. T. Structure and energetics of ligand binding to proteins: Escherichia coli dihydrofolate reductase - trimethoprim, a drug - receptor system. *Proteins: Struct., Funct., Genet.* **1988**, *4*, 31-47.

for TOC only

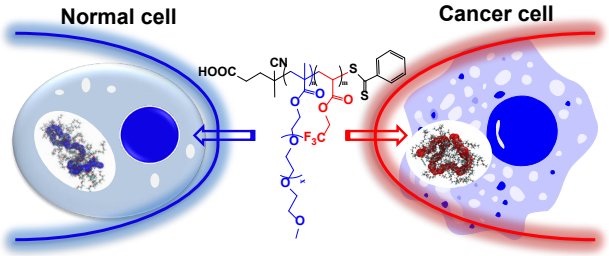
Normal cell
Cancer cell
HOOC
CN
S
S
O
O
O
O
O
O
$F_3C$